

## Intracellular MUC1 Peptides Inhibit Cancer Progression

Benjamin G. Bitler,<sup>2</sup> Ina Menzl,<sup>2</sup> Carmen L. Huerta,<sup>1</sup> Barbara Sands,<sup>1</sup> Wendy Knowlton,<sup>1</sup> Andrew Chang,<sup>1</sup> and Joyce A. Schroeder<sup>1,2,3</sup>

**Abstract Purpose:** During cancer progression, the oncoprotein MUC1 binds  $\beta$ -catenin while simultaneously inhibiting the degradation of the epidermal growth factor receptor (EGFR), resulting in enhanced transformation and metastasis. The purpose of this study was to design a peptide-based therapy that would block these intracellular protein-protein interactions as a treatment for metastatic breast cancer.

**Experimental Design:** The amino acid residues responsible for these interactions lie in tandem in the cytoplasmic domain of MUC1, and we have targeted this sequence to produce a MUC1 peptide that blocks the protumorigenic functions of MUC1. We designed the MUC1 inhibitory peptide (MIP) to block the intracellular interactions between MUC1/ $\beta$ -catenin and MUC1/EGFR. To allow for cellular uptake we synthesized MIP adjacent to the protein transduction domain, PTD4 (PMIP).

**Results:** We have found that PMIP acts in a dominant-negative fashion, blocking both MUC1/ $\beta$ -catenin and MUC1/EGFR interactions. In addition, PMIP induces ligand-dependent reduction of EGFR levels. These effects correspond to a significant reduction in proliferation, migration, and invasion of metastatic breast cancer cells *in vitro*, and inhibition of tumor growth and recurrence in an established MDA-MB-231 immunocompromised (SCID) mouse model. Importantly, PMIP also inhibits genetically driven breast cancer progression, as injection of tumor-bearing MMTV-pyV mT transgenic mice with PMIP results in tumor regression and a significant inhibition of tumor growth rate.

**Conclusions:** These data show that intracellular MUC1 peptides possess significant antitumor activity and have important clinical applications in the treatment of cancer.

MUC1 (DF3, CD227, episialin, PEM) is a heavily O-glycosylated heterodimeric protein of >300 kDa, normally expressed abundantly on the apical surface of glandular epithelia. In more than 90% of human breast carcinomas and metastases, apical localization is lost and MUC1 is overexpressed (by >10-fold) and underglycosylated (1, 2). Deregulated expression of MUC1 is found in many other types of adenocarcinomas as well, including cancers of the lung, pancreas, ovary, and prostate, in addition to being highly expressed in leukemias, myelomas, and lymphomas (3–5). Studies in both genetic mouse models and cell line models have shown that MUC1 is an oncogene. A transgenic mouse model driving MUC1 (human) overexpression to the mouse

mammary gland (MMTV-MUC1) results in the development of breast cancer and is accompanied by a failure of the mammary gland to undergo complete postlactational regression via apoptosis (6). Transfection of MUC1 into 3Y1 fibroblasts induces their transformation, and transfection of MUC1 into colon cancer cells shows that MUC1 overexpression inhibits drug-induced apoptosis (7).

The cytoplasmic domain of MUC1 contains sites for multiple protein interactions, although these interactions go largely unformed in the polarized epithelium of the normal breast, as the binding partners of MUC1 are typically found on the basolateral membrane (reviewed in refs. 8–10). During cancer progression, when there is a loss of cellular polarization, MUC1 is overexpressed and functionally interacts with src, GSK3 $\beta$ , epidermal growth factor receptor (EGFR), and  $\beta$ -catenin, among others (9, 11, 12). The sites for interaction between MUC1 and these proteins have been mapped to distinct domains within the 72-amino acid cytoplasmic tail of MUC1 (11, 13–15). Both EGFR and src can phosphorylate MUC1 on a YEKV motif, and this phosphorylation results in increased binding of MUC1 to  $\beta$ -catenin through an SAGNGGSSLS domain (11). Recent evidence shows that the interaction between MUC1 and EGFR can significantly modulate EGFR biology and effect EGFR-dependent transformation (9, 10).

It has been established in both human breast cancer cell lines and transgenic mice overexpressing MUC1 (MMTV-MUC1) that MUC1 and EGFR biochemically interact, resulting in the

**Authors' Affiliations:** <sup>1</sup>Department of Molecular and Cellular Biology, <sup>2</sup>Arizona Cancer Center, and <sup>3</sup>Bio5 Institute, University of Arizona, Tucson, Arizona  
Received 7/8/08; revised 9/8/08; accepted 9/9/08.

**Grant support:** Arizona Biomedical Research Corporation (J.A. Schroeder), the National Cancer Institute (J.A. Schroeder, B.G. Bitler, and I. Menzl), and the BIO5 Institute (J.A. Schroeder).

The costs of publication of this article were defrayed in part by the payment of page charges. This article must therefore be hereby marked *advertisement* in accordance with 18 U.S.C. Section 1734 solely to indicate this fact.

**Note:** Supplementary data for this article are available at Clinical Cancer Research Online (<http://clincancerres.aacrjournals.org/>).

**Requests for reprints:** Joyce A. Schroeder, Molecular and Cellular Biology, Arizona Cancer Center, PO Box 245024, Tucson, AZ 85724-5024. Phone: 520-626-1384; Fax: 520-626-3764; E-mail: jschroeder@azcc.arizona.edu.

©2009 American Association for Cancer Research.

doi:10.1158/1078-0432.CCR-08-1745

### Translational Relevance

The peptide-based therapy presented in this research describes a novel approach of targeting cancer-specific protein-protein interactions. The targets of MUC1 inhibitory peptides synthesized with the protein transduction domain PTD4 (PMIP), i.e., MUC1, EGFR, and  $\beta$ -catenin, are all clinically relevant and act together to play an important role in the progression of breast cancer. We have shown PMIP's ability to slow the proliferation and invasion of human breast cancer cells. Additionally, PMIP displayed efficacy in both transgenic and xenograft mouse models of breast cancer. In both of these mouse models PMIP was able to significantly slow the growth of primary tumors and reduce the amount of regrowth following tumor resection. All of these results indicate that PMIP has significant clinical implications in the treatment of breast cancer.

potentiation of epidermal growth factor (EGF)-dependent p42/44 ERK activation during lactation (11, 16). Recently, our laboratory has shown that MUC1 expression inhibits the ligand-mediated ubiquitination and degradation of EGFR while enhancing its internalization and recycling (9). To evaluate the role of Muc1 in transformation, we further generated whey acidic protein-transforming growth factor  $\alpha$  (WAP-TGF $\alpha$ ) mice on a Muc1 null background that revealed that Muc1 expression has a dominant effect on TGF $\alpha$ -dependent transformation of the breast, promoting both onset and progression (10).

Although it is now established that EGFR is potentially regulated by MUC1 expression, transgenic mouse models have also implicated the cell adhesion protein,  $\beta$ -catenin, in EGFR and MUC1 signaling. In a study of the WAP-TGF $\alpha$  transgenic model, Wnt1 and Wnt3 were found to be selectively activated in the most aggressive breast tumors (17). The Wnts are secreted glycoproteins that bind the transmembrane frizzled receptor, resulting in a signaling cascade that inactivates the mechanism for  $\beta$ -catenin degradation and results in transformation (18–23). Additionally, in MMTV-Wnt1 transgenic mice, EGFR was found to interact with and phosphorylate  $\beta$ -catenin in a tumor-specific manner (24). These studies show that  $\beta$ -catenin and EGFR can affect their respective pathways to promote transformation. Finally, MUC1 is also implicated in  $\beta$ -catenin-dependent transformation, indicating that these three proteins have the ability to cooperatively promote cancer progression. In MMTV-Wnt1 transgenic mouse models crossed onto a Muc1 null background, loss of Muc1 corresponds to a significant reduction in tumor progression (12). In a subsequent study, interactions between MUC1 and  $\beta$ -catenin were found to be highly increased in samples from human metastatic breast tumors, indicating that these interactions are clinically relevant (12).

Together, these studies show the strong potential for MUC1, EGFR, and  $\beta$ -catenin to affect each other during transformation, including their striking co-up-regulation during transformation and metastasis. MUC1 can inhibit the down-regulation of EGFR and promote the transforming ability of both EGFR and  $\beta$ -catenin. Additionally, genetically derived mouse models implicate MUC1 in both EGFR- and  $\beta$ -catenin-dependent transformation and metastasis. Interestingly, the interaction

sites on MUC1 for both EGFR and  $\beta$ -catenin lie in tandem in the MUC1 cytoplasmic domain. This study shows that targeting the interaction domain of MUC1 for both EGFR and  $\beta$ -catenin through the utilization of MUC1 dominant-negative peptides can significantly affect breast cancer progression. Importantly, this dominant-negative peptide can significantly inhibit tumor progression in a genetically driven mouse model of breast cancer over a relatively short treatment time and may have important clinical applications.

### Materials and Methods

**Cell culture.** Metastatic breast cancer cell lines BT20 and MDA-MB-231 cells were obtained from the American Tissue Culture Collection. These cell lines were cultured with 10% Fetal Bovine Serum (FBS; Cellgro), 1% penicillin-streptomycin-glutamine (Invitrogen), and Eagle's minimal essential medium (EMEM; BT20; American Tissue Culture Collection) media or RPMI 1640 (MDA-MB-231; Cellgro) at 37°C with 5% CO<sub>2</sub> in a humidified incubator.

**Invasion assay.** Collagen matrix (0.9 mg/mL Type I Rat tail collagen; BD Biosciences), 83.0% (v/v) M-199 medium (Life Technologies), and 0.18% NaHCO<sub>3</sub> (Fisher) were poured into a 96-well plate. Prior to collagen polymerization, a 8.0- $\mu$ m pore transwell insert (Corning Inc.) was placed on top of the matrix. The polymerized collagen was rehydrated using a chemoattractant (20% FBS/EMEM). BT-20 cells were treated with 10  $\mu$ mol/L of human MUC1 inhibitory peptide synthesized with the protein transduction domain PTD4 (hPMIP), control peptide (CP), PTD4 peptides, or water in serum-free EMEM media overnight. Prior to loading the cells onto the transwell inserts they were fluorescently labeled with Calcein-AM (Invitrogen) for 30 min and then washed with PBS. The cells were then resuspended in a 10  $\mu$ mol/L peptide/EMEM serum-free media and loaded onto the inserts in each well (15,000 cells/well). The cells were allowed to invade into the matrix for 10 h at 37°C with 5% CO<sub>2</sub> in a humidified incubator. After 10 h, the collagen matrix was treated with a 0.25% collagenase in 40% FBS/PBS and the inserts were removed (Calbiochem). The number of fluorescently labeled cells that had invaded into the collagen were measured using a Molecular Devices spectrophotometer (Ex:485, Em:538, and Cutoff:530). For each treatment group, a set of cells was placed directly into the bottom chamber and used as a reference for 100% of cell invasion. Invasion is then indicated as percent invasion (invaded cells/total cells).

**MTT proliferation assay.** BT20 cells were plated into a 96-well plate ( $5 \times 10^3$  cells per well). The cells were allowed to adhere and then they were treated daily with 10  $\mu$ mol/L of hPMIP, CP, PTD4 peptides, or water (treatments diluted in 10% FBS/EMEM) for 7 d. After treatment the Vybrant MTT Cell Proliferation Assay (Molecular Probes) was done following the manufacturer's protocol.

**Immunoprecipitation and immunoblotting.** Protein was treated as described in (9).

**Densitometry.** Immunoblotting analysis was done as in (9).

**Antibodies and growth factors.** Anti-MUC1 (CT-2) and anti-EGFR (Ab-13) antibodies were purchased from Neomarkers Inc. Anti-MUC1 (H295) was purchased from Santa Cruz Biotechnology. The total Erk (9102) and phosho-EGFR (1173) were purchased from Cell Signaling. Antibodies against phosphorylated tyrosine (PY99), EGFR/erbB1 (1005), and  $\beta$ -catenin (C-18) were all purchased from Santa Cruz Biotechnologies. The  $\beta$ -catenin antibody used for immunofluorescence was from BD Scientific. The  $\beta$ -actin (AC-15) and dual-phosphorylated Erk (M-8159) antibodies were purchased from Sigma Chemical Company. Secondary antibodies conjugated to horseradish peroxidase (HRP) were acquired from Molecular Probes (Invitrogen) and the antihamster HRP conjugated antibody was purchased from Jackson Labs. The secondary antibodies, donkey antimouse 488 and donkey antirabbit 594 were purchased from Molecular Probes

(Invitrogen). EGF was stored at  $-20^{\circ}\text{C}$  at a concentration of  $100\text{ ng}/\mu\text{L}$  (Invitrogen).

**Immunofluorescence.** For peptide uptake, BT20 cells were treated for 4 h with  $10\text{ }\mu\text{mol}/\text{L}$  hPMIP tagged with biotin and fixed in 1:1 acetone:methanol. Fixed cells were treated with an anti-streptavidin-488 antibody and washed with  $0.02\%$   $\text{NaN}_3/\text{PBS}$  and incubated with Slowfade Gold antifade reagent with 4',6-diamidino-2-phenylindole (DAPI; Invitrogen). Cells were visualized with a fluorescence DMLB Leica compound microscope. For  $\beta$ -catenin/MUC1, BT-20 cells were incubated with  $10\text{ }\mu\text{mol}/\text{L}$  of hPMIP, CP, PTD4, or water. The immunostaining of the cells was done as in (9). Cells were visualized with a fluorescence Zeiss confocal microscope.

**Peptide synthesis.** The hPMIP, biotin-hPMIP, mouse PMIP (msPMIP), FITC-msPMIP, CP, and PTD4 polypeptides were synthesized by GenScript and delivered lyophilized. The peptides were resuspended at a concentration of  $500\text{ }\mu\text{mol}/\text{L}$  in water and stored at  $-80^{\circ}\text{C}$  in single-use aliquots. Peptide sequences are shown in Fig. 1A.

**Human breast tumor xenografts.** Immunocompromised (scid) mice (Taconic) were tested for the presence of serum IgG and found to be  $<20\text{ }\mu\text{g}/\text{mL}$  IgG. Female mice (4 to 6 weeks old) were injected with  $1 \times 10^7$  cells embedded in Matrigel (BD Biosciences) into the mammary fat pad and allowed to grow to either  $100\text{ mm}^3$  or  $500\text{ mm}^3$ , based on the formula  $a^2 \times b/2$  where  $a$  is the smaller diameter and  $b$  is the larger diameter. Mice were injected i.p. with  $50\text{ }\mu\text{g}/\text{g}$  body weight of either hPMIP or PTD4 control peptide for 21 d and measured with calipers every 2 d. Either at the end of 21 d or after the tumor had reached  $800\text{ mm}^3$ , tumors were resected by injecting the mice with buprenorphine ( $2.5\text{ mg}/\text{kg}$  body weight; Infusion Solutions) at least 1 h prior to resection and anesthetizing the mice with isoflurane (Abbott). Following surgery, the mice were treated with buprenorphine ( $2.5\text{ mg}/\text{kg}$  body weight) 8 and 16 h postsurgery. The animals were followed for 10 d to examine regrowth at the primary tumor site or at secondary mammary glands, then sacrificed.

**Transgenic mice.** MMTV-pyV mT mice on an FVB background (W. Muller, ref. 25, obtained from Jackson Laboratories) entered into study upon the development of tumors that measured  $>0.5\text{ cm}$  in at least one diameter. Only mice age  $>7\text{ wk}$  were included in the study and mice that developed fluid cysts were excluded. Animals were injected i.p. with  $50\text{ }\mu\text{g}/\text{g}$  body weight of msPMIP or PTD4 once daily for 21 d. Each of 10 mammary glands were measured using calipers every 2 d, and measurements were used to determine tumor volume based on the

formula  $a^2 \times b/2$ , with  $a$  being the smaller diameter and  $b$  being the larger diameter. After treatment for 21 d, the mice were sacrificed by  $\text{CO}_2$  inhalation and the tissues resected. Several msPMIP-treated mice were injected with FITC-msPMIP ( $50\text{ }\mu\text{g}/\text{g}$  body weight) 1 or 4 h prior to sacrifice and intact tissues were visualized using a fluorescence MZFLIII Leica dissection microscope.

Both the xenograft and transgenic mouse studies were done by the Experimental Mouse Shared Service at the Arizona Cancer Center (University of Arizona, Tucson) under protocols approved by the Institutional Animal Care and Use Committee of the University of Arizona.

**Tissue analysis.** Tumor tissues from the xenograft and transgenic mouse models were fixed in  $10\%$  buffered formalin and stored in  $70\%$  ethanol. Tissues were paraffin-embedded, sectioned, and subsequently used for H&E staining and caspase-3 immunohistochemistry. Tissue embedding, sectioning, H&E staining, and cleaved caspase-3 immunohistochemistry were all done by the Tissue Acquisition and Cellular Molecular Analysis Shared Service at the Arizona Cancer Center.

**Statistical analysis.** All statistics were done in Excel (Microsoft).

## Results

**PMIP efficiently enters the cells, reduces EGFR protein levels and inhibits MUC1 colocalization with  $\beta$ -catenin.** The MUC1 cytoplasmic domain is composed of 72 amino acids, within which lies a 15-amino acid domain containing sites of EGFR phosphorylation (human = YEKV and mouse = YEEV) and  $\beta$ -catenin binding (human = SAGNGGSSLS and mouse = SAGNGSSLS, Fig. 1A; refs. 11, 26). We synthesized a 15-amino acid peptide to determine if it could act in a dominant-negative fashion to block interactions between endogenous MUC1 and EGFR/ $\beta$ -catenin. To allow this peptide to gain entrance to the cell, we synthesized it in tandem with a protein transduction domain (PTD4, Fig. 1A; ref. 27, reviewed in ref. 28). To show that PMIP was entering the cells, we pulsed cells *in vitro* with a biotin-labeled hPMIP ( $10\text{ }\mu\text{mol}/\text{L}$ ) peptide (biotin-hPMIP). We found that the peptide was taken up and is retained in BT20 breast cancer cells (Fig. 1B).

To determine if the hPMIP peptide was able to block the interaction between EGFR and MUC1, we treated BT20 cells

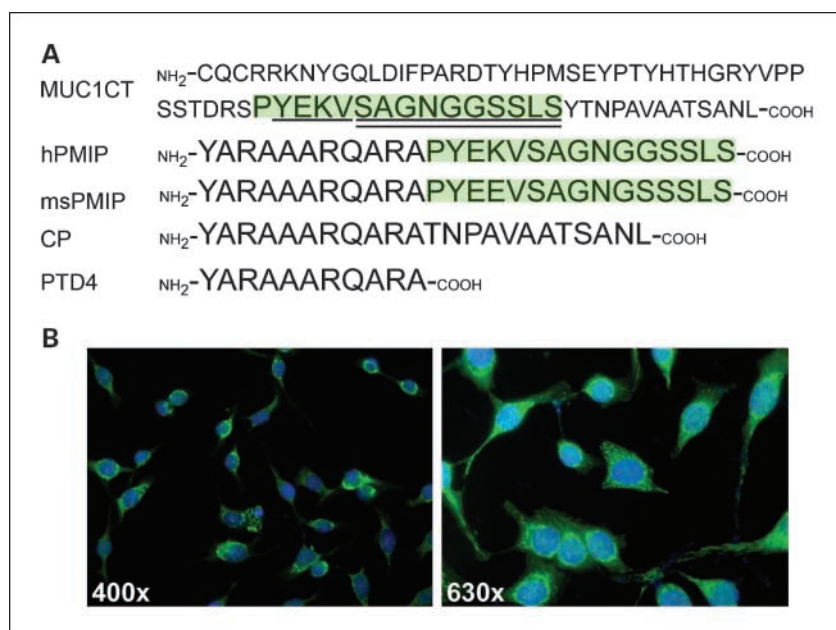


**Fig. 1.** A MUC1 peptide (PMIP) can efficiently enter cells. **A**, MUC1's cytoplasmic amino acid sequence (MUC1CT), which includes an EGFR phosphorylation site (underlined) and  $\beta$ -catenin binding site (double underlined). Human (hPMIP) and mouse (msPMIP) sequence for the PMIP peptide, the PTD4 protein transduction domain, and the control peptide (CP) containing the last 12 amino acids of the human MUC1 cytoplasmic domain are shown. **B**, BT-20 cells were treated with  $10\text{ }\mu\text{mol}/\text{L}$  biotin-hPMIP for 4 h. Green, biotin-PMIP; blue, DAPI (nucleus),  $400\times$  and  $630\times$ .

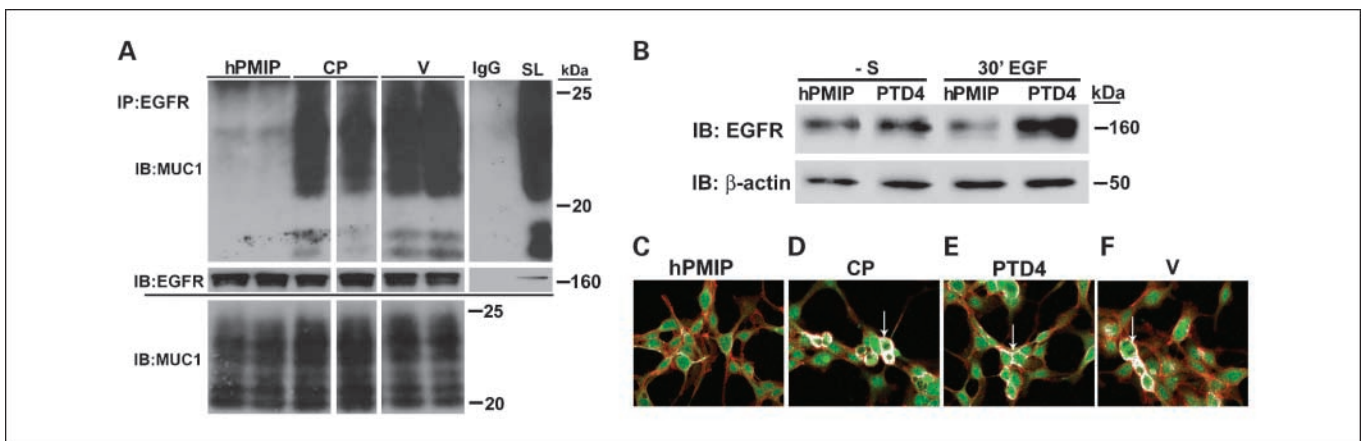


**Fig. 2.** PMIP blocks MUC1/ $\beta$ -catenin and MUC1/EGFR interactions. **A.** BT-20 cells were treated overnight (-serum) with either 10  $\mu$ mol/L hPMIP, 10  $\mu$ mol/L CP, or vehicle control (water; V), and protein lysates generated. Lysates (500  $\mu$ g) were immunoprecipitated with either anti-EGFR (Ab-13; lanes 1-6, top and middle panel) or IgG (lane 7, top and middle panel) and immunoblotted with anti-MUC1 (top panel; CT2) or anti-EGFR (middle panel; 1005). Total levels of MUC1 (35  $\mu$ g) are shown in the bottom panel and in right column of top panel (straight lysate, SL). White lines through blots indicate same gel and exposure but were noncontiguous. **B.** BT-20 cells were treated for 18 h (-S) with hPMIP (10  $\mu$ mol/L) or PTD4 (10  $\mu$ mol/L). The cells were treated with EGF (30' EGF, 10 ng/mL) to induce endocytosis or left serum-free (-S) and protein lysates were generated. The lysates were immunoblotted for EGFR (1005) and  $\beta$ -actin (AC-15). **C to F.** BT-20 cells were treated (-serum) overnight with (C) hPMIP (10  $\mu$ mol/L), (D) CP (10  $\mu$ mol/L), (E) PTD4 (10  $\mu$ mol/L), or (F) water (V) and pulsed with the same peptides for an additional 30' prior to fixation. The cells were probed for MUC1 (primary; H295; red) and  $\beta$ -catenin (primary; C-14; green). Colocalization (arrows) is designated with white pixels. Magnification, 400 $\times$ .

overnight with either 10  $\mu$ mol/L hPMIP, 10  $\mu$ mol/L CP, or peptide vehicle, immunoprecipitated EGFR and immunoblotted for MUC1 (Fig. 2A). Although we were able to detect coimmunoprecipitation between MUC1 and EGFR in control-treated cells, interaction was significantly reduced in hPMIP-treated cells (Fig. 2A, top panel). In addition to protein interaction, we had previously shown that MUC1 expression inhibits the EGF-dependent degradation of EGFR (9). To determine if PMIP was able to block the MUC1-mediated effects on EGFR degradation, we treated BT20 and MDA-MB-231 cells with hPMIP or PTD4 control, and induced EGFR endocytosis by treatment with EGF for 30 minutes. Examination of EGFR protein levels by immunoblotting showed that hPMIP treatment resulted in a reduction of EGFR levels following EGF treatment (Fig. 2B and data not shown). Note that in the absence of EGF treatment, hPMIP treatment does not affect EGFR levels.

To determine if PMIP could block those interactions between MUC1 and  $\beta$ -catenin that occur during transformation, we examined the effects of hPMIP treatment on protein colocalization in the BT-20 breast cancer cell line (12, 24). Cells were serum-starved and treated with either 10  $\mu$ mol/L hPMIP, 10  $\mu$ mol/L CP, 10  $\mu$ mol/L PTD4, or vehicle control overnight, fixed, and immunofluorescence was done. Although  $\beta$ -catenin and MUC1 colocalization at the cell cortex could be identified in control conditions (Fig. 2C-F, arrows), their interactions were significantly inhibited by hPMIP treatment (Fig. 2C).

These results show that PMIP treatment inhibits both MUC1/ $\beta$ -catenin and MUC1/EGFR interactions. In addition, PMIP inhibits MUC1-mediated inhibition of EGF-dependent degradation of EGFR.

**PMIP inhibits cellular invasion and proliferation in vitro.** As hPMIP treatment showed a strong biochemical inhibition of MUC1 interactions with both  $\beta$ -catenin and EGFR, we next examined the potential effects of treatment on cell growth and invasion. To determine the effects of PMIP treatment on cell proliferation, BT20 cells were treated with either 10  $\mu$ mol/L

hPMIP, 10  $\mu$ mol/L CP, 10  $\mu$ mol/L PTD4, or peptide vehicle for 7 days continually, then the number of cells was evaluated by quantifying the differences in formazan conversion through a colorimetric MTT assay (29). Following 7 days of hPMIP treatment we observed that the growth of BT20 cells was significantly inhibited compared with CP, PTD4, and water (V; \*,  $P < 0.001$ , \*\*,  $P < 0.0002$ , \*\*\*,  $P < 0.002$ , Fig. 3A).

We next evaluated the effect of PMIP on cellular invasion. BT20 or MDA-MB-231 breast cancer cells were treated overnight with either hPMIP or PTD4 control peptide (10  $\mu$ mol/L), then induced to invade through an 8.0- $\mu$ m filter into Type I collagen using 20% FBS as a chemoattractant. Cells that were able to migrate through the filter and invade into the gels were fluorescently labeled and quantified. We found that PMIP treatment significantly inhibited the ability of cells to invade compared with cells treated with controls in both BT-20 cells and MDA-MB-231 ( $^{\#}P < 0.0001$  and data not shown; Fig. 3B).

**PMIP inhibits tumor growth and inhibits recurrence in a xenograft breast cancer model.** As hPMIP strongly inhibited cellular growth and invasion *in vitro*, we next evaluated the ability of hPMIP to suppress tumor growth and metastasis *in vivo*. In these experiments, highly metastatic MDA-MB-231 breast cancer cells were implanted into the mammary fat pad of scid mice and tumor growth was evaluated.

To determine the potential effects of hPMIP on primary tumor growth, scid mice bearing MDA-MB-231 tumors (100 mm<sup>3</sup>) were treated for 21 days with either hPMIP or PTD4 control peptide (i.p. injections; Fig. 4A to C). Upon removal of drug, tumors were allowed to continue to grow until they reached a volume of 1,000 mm<sup>3</sup>, then surgical resection of primary tumors was done (Fig. 4B). Treatment with hPMIP resulted in a significant decrease in tumor size compared with control-treated animals at 21 days when drug administration was stopped ( $^*P = 0.028$ , Fig. 4A). Additionally, this corresponded to a significant increase in the length of time required for hPMIP-treated mice to reach resection size of 1,000 mm<sup>3</sup> ( $^{**}P = 0.03$ ; Fig. 4B). Although treatment

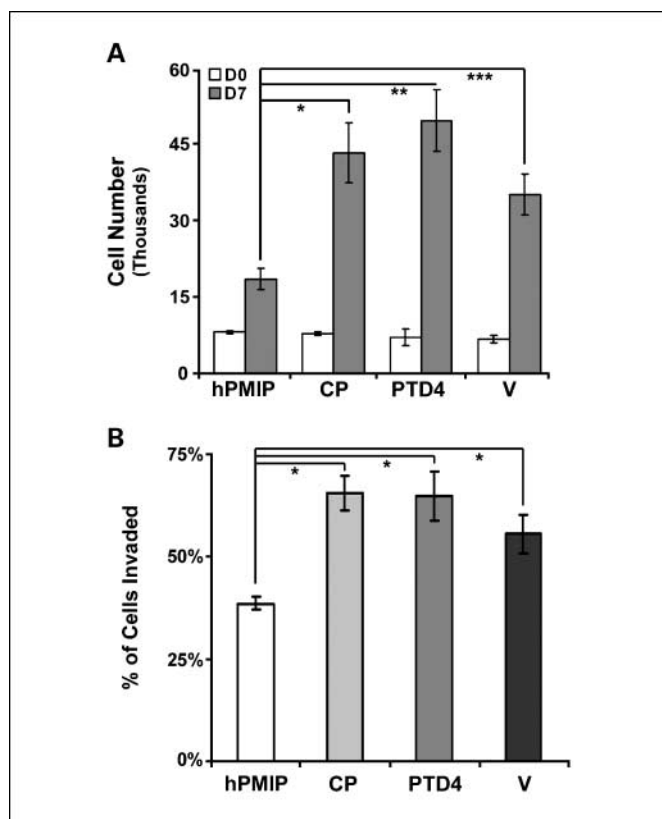


**Fig. 3.** PMIP inhibits cell proliferation and invasion of breast cancer cells *in vitro*. **A**, BT20 cells were cultured in a 96-well dish ( $5 \times 10^3$  cells/well) and treated daily for 7 d with either hPMIP (10  $\mu$ mol/L), CP (10  $\mu$ mol/L), PTD4 (10  $\mu$ mol/L), or water (V) in EMEM 10% FBS. An MTT assay was done to quantify cell number at the start of treatment (day 0, DO) and after treatment was complete (day 7, D7). \*,  $P < 0.001$ ; \*\*,  $P < 0.0002$ ; \*\*\*,  $P < 0.0001$ , ANOVA. Error bars, SE. **B**, BT-20 cell lines were treated with either hPMIP (10  $\mu$ mol/L), CP (10  $\mu$ mol/L), PTD4 (10  $\mu$ mol/L), or water (V) overnight, labeled with calcein AM, allowed to invade through a transwell (8.0  $\mu$ m) insert into a type I collagen gel, and the invaded cells were fluorescently measured. (## $P < 0.0001$ , ANOVA). The data from the invasion and proliferation assays represent four independent experiments with at least seven replicates per experiment. Error bars, SD.

ended approximately 20 days prior to resection, we observed that hPMIP treatment substantially decreased the amount of tumor regrowth and spread 10 days after resection (Fig. 4C). We also noted a decrease in the size of metastatic tumors in the hPMIP-treated animals compared with control, and next designed an experiment that would allow us to determine if hPMIP was affecting tumor spread following tumor resection.

To evaluate the effects of PMIP on tumor spread (Fig. 4A and B), MDA-MB-231 breast cancer cells were allowed to establish a large tumor mass (500  $\text{mm}^3$ ) and mice were injected (i.p.) for 21 days with hPMIP or control peptide (PTD4; Fig. 4D). Immediately after the end of treatment, primary breast tumors were resected, and animals were followed to examine rates of tumor regrowth and/or metastasis to secondary mammary glands. Whereas the presence of secondary mammary gland tumors were found in equal number for both treatment groups, the tumor volume for the control-treated animals averaged 760  $\text{mm}^3$  and the PMIP-treated averaged only 73  $\text{mm}^3$  (Fig. 4E). Note that mice were not treated with drug during the 10 days in which regrowth was followed. These xenograft models revealed that PMIP

treatment could have long lasting antigrowth effect, which was observed in tumor regrowth following resection.

**PMIP inhibits tumor growth and induces regression in genetically driven breast cancer.** Although the xenograft model showed the effect of hPMIP treatment on growth and progression of established cell lines, we wanted to determine how msPMIP would affect tumor initiation and progression in a mouse model that better recapitulates human breast cancer. The MMTV-pyV mT transgenic mouse model of breast cancer strongly resembles human breast cancer by activating multiple signaling pathways, including AKT, src, and shc (25, 30). Studies have shown that the resulting breast cancer pathologically and molecularly mimics the full progression of hyperplasia, ductal carcinoma *in situ*, and adenocarcinomas observed in human disease (31, 32). To first determine if peptide could be delivered to the mammary glands and tumors of these animals, we injected FITC-labeled msPMIP and analyzed peptide retention (Fig. 5A). At two hours postinjection, FITC was detected throughout the animal's body cavity, including all organs (data not shown). After four hours, FITC-msPMIP was found to be retained selectively in the mammary gland, mammary gland tumors, and the colon and skin (Fig. 5A and data not shown).

To determine the effects of msPMIP on genetically driven breast cancer progression, MMTV-pyV mT mice bearing at least one mammary gland tumor of  $>0.5$  cm in diameter (in MMTV-pyV mT mice there are 10 potential tumor sites) were treated for 21 days with either msPMIP or PTD4 control peptide. Treatment had a dramatic effect on tumor growth, as msPMIP significantly slowed the total tumor growth from  $\sim 590\%$  to  $\sim 194\%$  over the 21 days of treatment (\* $P = 0.039$ ; Fig. 5B). Additionally, msPMIP treatment significantly decreased the tumor growth rate compared with control (PTD4)-treated tumors (\*\* $P = 0.007$ ; Fig. 5C). Note that treatment of MMTV-pyV mT mice with hPMIP (as opposed to msPMIP) had no effect on tumor growth, emphasizing the amino acid specificity of PMIP.

We next analyzed the overall size of tumors that arose throughout the study. This analysis shows that whereas 13% of the tumors in the control (PTD4) group grew larger than 500  $\text{mm}^3$  by the end of the study, only 1% of the tumors in the msPMIP-treated group reached that size (Fig. 5D). As this transgenic model had continual expression of the polyoma middle T transgene driving tumorigenesis throughout the study, we next examined the effects of drug treatment on the formation of new tumors. Although both msPMIP and control (PTD4) groups had a similar number of tumors sized 100 to 300  $\text{mm}^3$  at the beginning of treatment, this number nearly doubled by the end of treatment in the control group, but remained similar in the msPMIP group (Fig. 5D). These data indicated that msPMIP treatment inhibits tumor initiation in this model (initiation equals percent of tumor transitions from 0  $\text{mm}^3$  to 100  $\text{mm}^3$ ). To analyze tumor initiation further, we evaluated the percent of tumors that were initiated during drug treatment. This analysis shows that in the msPMIP group there was a significant decrease (12 versus 20 initiated tumors, data not shown;  $P = 0.0045$ ) of tumor initiation during the study.

Although highly significant decreases in tumor formation and growth were observed from the treatment of tumor-bearing MMTV-pyV mT mice with msPMIP, not all tumors in the study

responded to treatment (Fig. 6A). Analysis of each mammary gland showed that although most tumor growth rates slowed substantially in response to msPMIP (white bars), a number of tumors continued to grow, indicative of the stochastic pathway activation in this model. Importantly, a subset of established tumors treated with msPMIP (four tumors) regressed completely under treatment, although none of the control-treated tumors did so (Fig. 6A, \*). In addition, there was no detectable toxicity (no weight loss, organ failure, or disorientation) following treatment with msPMIP or PTD4. Further investigation of tumor tissue sections by cleaved caspase-3 immunohistochemistry and H&E staining of tumors that regressed or responded to msPMIP treatment did not reveal a difference in apoptotic cells compared with PTD4 control peptide-treated tumors (Fig. 6B).

**Mouse PMIP treatment results in a reduction of EGFR and Muc1 levels.** To determine if msPMIP was affecting EGF-dependent degradation of EGFR *in vivo*, we generated protein lysates from tumors of MMTV-pyV mT animals injected with EGF and peptide 30 minutes prior to animal sacrifice (after a standard 21-day drug treatment). We observed a striking reduction in the expression of EGFR and corresponding phosphotyrosine in the msPMIP-treated mouse compared with the control-treated animal (Fig. 7A). Note that in this mouse, there were no frank tumors remaining after the 21-day msPMIP treatment (remaining mammary fat pads were analyzed), whereas we obtained six tumors of >400 mm<sup>3</sup> from control-treated animals. Analysis of EGFR expression and activation of

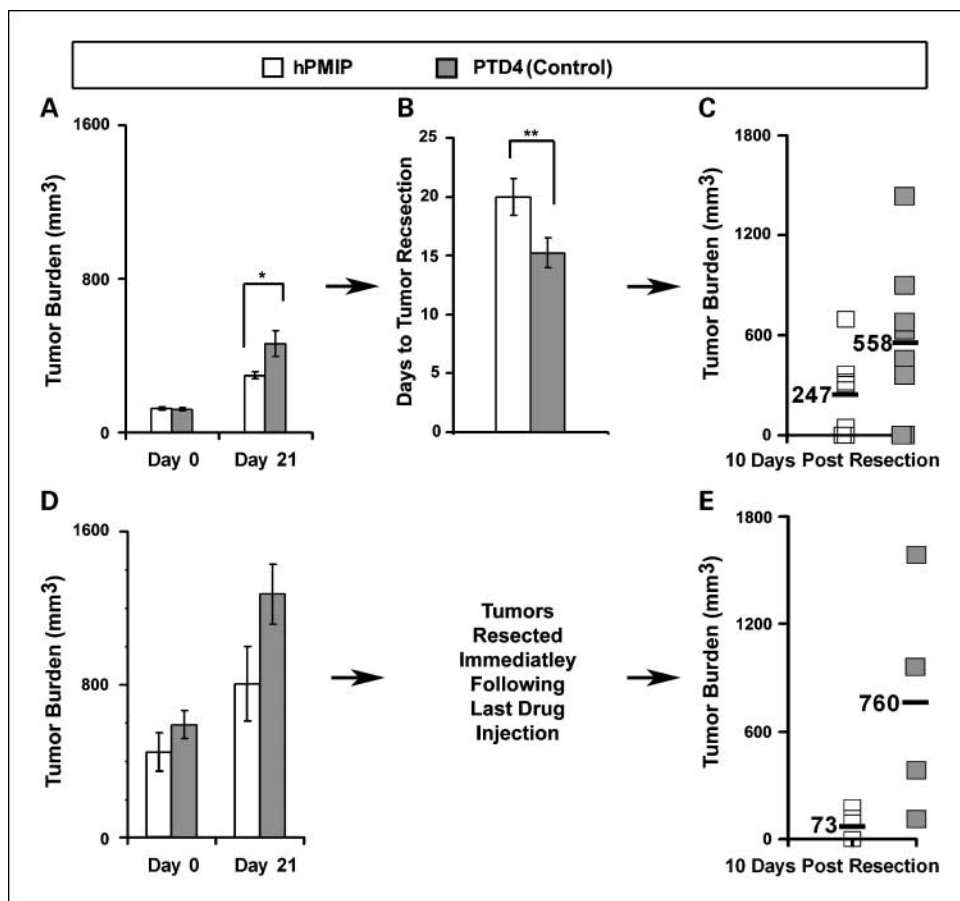
the MDA-MB-231 xenograft tumors was restricted to tumors that were not treated with EGF. Nonetheless, we did observe a slight reduction in the levels of phospho-EGFR (Y1173) in hPMIP-treated compared with control-treated tumors (Supplementary Fig. S1, top panel). Tyrosine 1173 phosphorylation can result in the recruitment of shc to EGFR, resulting in activation of the mitogen-activated protein kinase ERK. We therefore examined activation of ERK, and found that hPMIP treatment resulted in a strong down-regulation of ERK activity compared with controls (Supplementary Fig. S1).

To determine if msPMIP blocked interaction between Muc1 and  $\beta$ -catenin, we began by establishing levels of Muc1 protein expression in the tumor lysates. Interestingly, we found that msPMIP treatment induced a loss of Muc1 protein in both the MMTV-pyV mT model (Fig. 7A and B) and in the MDA-MB-231 xenograft model (Fig. 7C and D). Total levels of  $\beta$ -catenin and its target genes cyclin D1 and Twist were unchanged between PMIP and control (data not shown).

### Discussion

We report here that a MUC1 mimetic peptide (MIP) linked to a protein transduction domain (PTD4) can freely enter transformed cells and inhibit their invasion *in vitro*. This same peptide can inhibit primary tumor growth, tumor spread, and recurrence of tumors after resection in an orthotopically implanted breast cancer model. PMIP can survive in circulation with tissue-specific retention and no detectable toxicity. Importantly, PMIP

**Fig. 4.** PMIP significantly inhibits tumor growth and recurrence *in vivo*. **A**, MDA-MB-231 cells in Matrigel were injected into the mammary fat pad of scid mice, and daily peptide treatment (50  $\mu$ g/g body weight of hPMIP or PTD4) began when tumors reached 100 mm<sup>3</sup> (hPMIP and PTD4, *n* = 8 mice) and primary tumor growth was assessed (\*, *P* = 0.028, ANOVA). Tumor burden represents the average volume ( $v = a^2 \times b/2$ ) of all tumors at the stage indicated. **B**, after the end of treatment, the amount of time the tumors took to progress to 1,000 mm<sup>3</sup> was measured (\*\*, *P* = 0.03, ANOVA). **C**, after resection, mice were observed for tumor regrowth at the primary site or secondary mammary glands (hPMIP, *n* = 7 mice; PTD4, *n* = 8 mice). **D**, MDA-MB-231 cells in Matrigel were injected into the mammary fat pad of scid mice, and daily peptide treatment (50  $\mu$ g/g of hPMIP or PTD4) began when tumors reached 500 mm<sup>3</sup> (hPMIP, *n* = 6 mice; PTD4, *n* = 4 mice) and primary tumor growth was assessed. **E**, following 21 d of treatment the tumors were resected immediately and tumor regrowth at the primary site and spread to secondary mammary glands was monitored (hPMIP, *n* = 4 mice; PTD4, *n* = 4 mice). Error bars, SE.



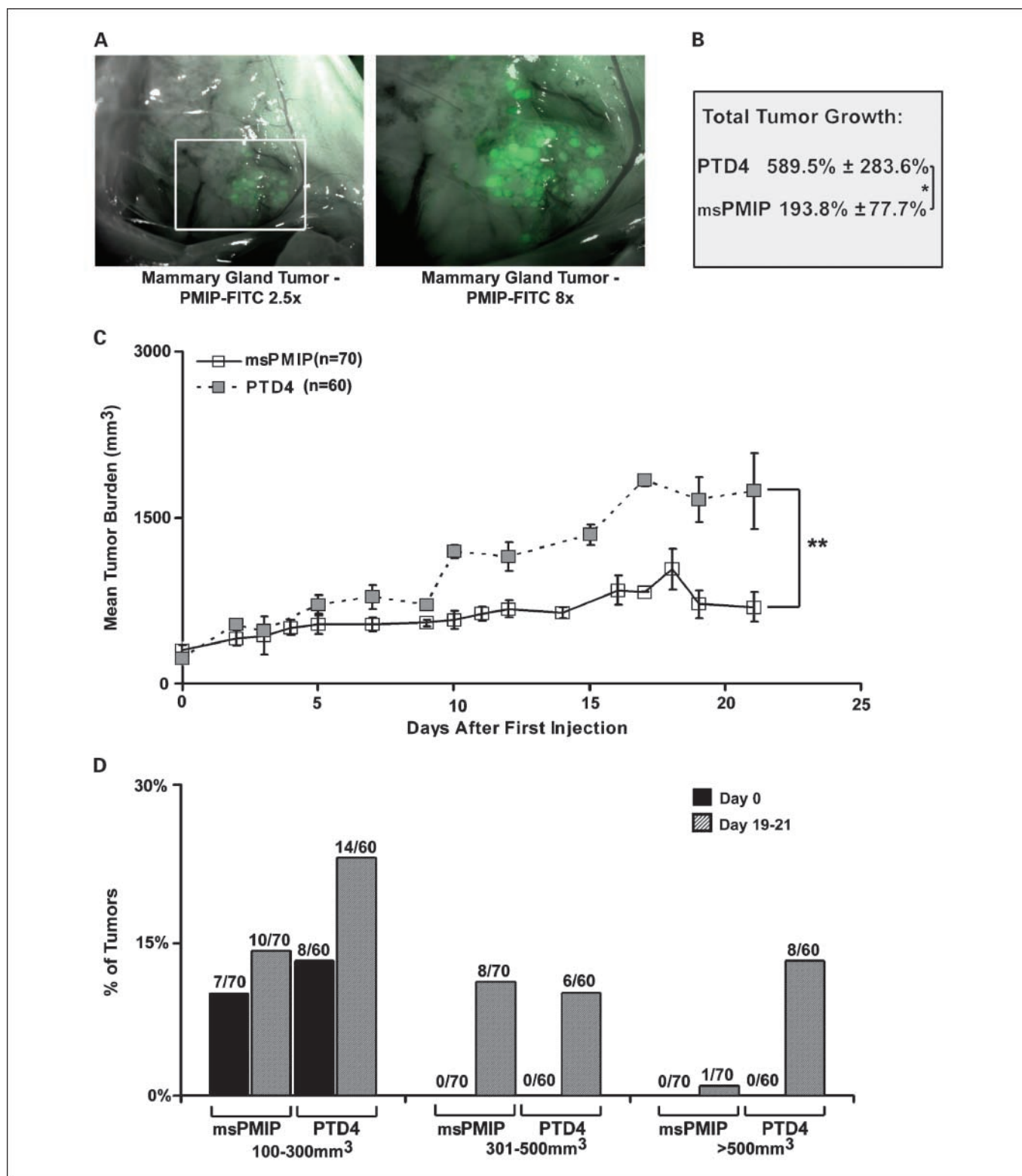


**Fig. 5.** PMIP significantly slows progression of MMTV-pyV nT-induced mammary gland tumors. **A**, MMTV-pyV nT transgenic mice were injected with FITC-msPMIP (50 µg/g body weight), sacrificed 4 h later, and various tissues visualized using fluorescence microscopy. FITC-msPMIP localization in the mouse mammary gland tumors is shown (2.5× and 8×). **B**, mammary gland tumors (>0.5 cm in diameter) were allowed to develop and mice were injected daily (50 µg/g body weight, 21-d treatment, i.p. injection, once per day) with either msPMIP (7 mice) or PTD4 (6 mice). At the end of treatment, animals were sacrificed and proteins lysates were made of the tumors for later analysis. In the course of treatment, total tumor growth for all tumor sites (msPMIP, *n* = 70; PTD4, *n* = 60) was significantly lower in the msPMIP-treated mice than in the PTD4 mice (193.8% ± 77.7% versus 589.5% ± 283.6%; \*, *P* = 0.039, ANOVA). **C**, mammary gland tumors of msPMIP-treated mice grew at a significantly slower rate than PTD4-treated tumors (\*\*, *P* = 0.0076, ANOVA). **D**, tumor size distribution for the msPMIP- or PTD4-treated transgenic mice revealed that 47% (28 out of 60 possible tumor sites) of the PTD4-treated tumors were larger than 100 mm<sup>3</sup> compared with 27% (19 out of 70 possible tumor sites) of the msPMIP-treated tumors. Numbers above data are numbers of tumors that meet the size criteria over the total potential tumor sites.

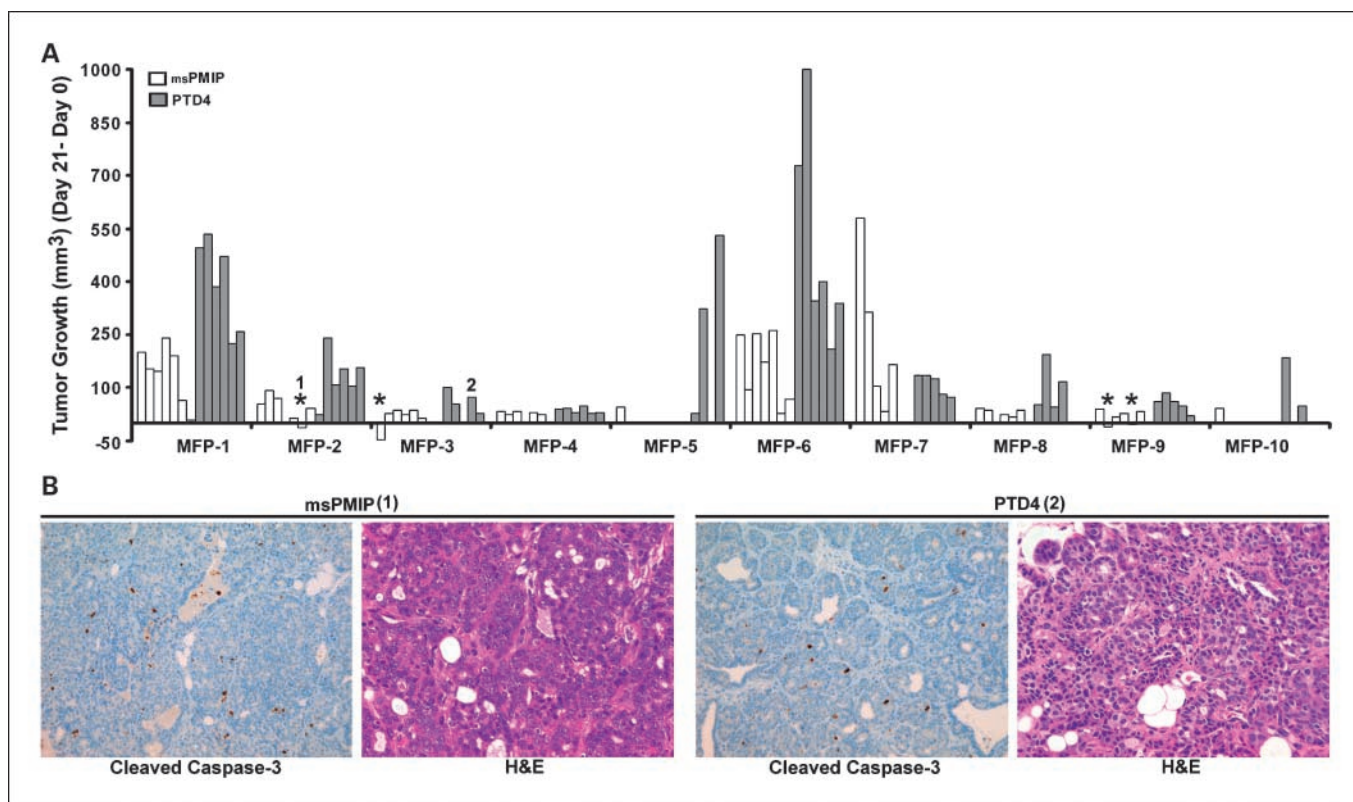


**Fig. 6.** MMTV-pyV mT tumors have differential response to msPMIP. *A*, individual growth of each tumor site (each bar is an individual tumor site) from animals described in Fig. 3 were treated daily with msPMIP (open bars) or PTD4 (grey bars) at 50  $\mu\text{g/g}$  body weight for 21 d. Tumor progression was observed every 3 d during the 21-d treatment (PTD4,  $n = 60$  tumor sites; PMIP,  $n = 70$  tumor sites). In four instances (\*), msPMIP treated tumors completely regressed, but none of the control (PTD4) treated tumors regressed. Individual tumor sites are grouped by mammary fat pads (1-10) to allow for the comparison of similar anatomic sites. MFP, mammary fat pad. *B*, tumors from mice treated with msPMIP (1, left 2 panels) and PTD4 (2, right 2 panels) were sectioned (3  $\mu\text{m}$ ) and subsequently used for H&E staining and cleaved caspase-3 immunohistochemistry (200 $\times$ ).

can significantly inhibit tumor growth in a genetically driven mouse model that mimics human breast cancer. Mechanistically, this tumor-inhibitory effect is closely associated with a decrease in EGFR and MUC1 expression. Together these data indicate that this peptide-based intracellular drug shows strong efficacy as a nontoxic treatment for breast cancer.

The overexpression of human MUC1 in mouse mammary glands promotes transformation, and the loss of MUC1 in several transgenic models can significantly delay tumor onset (6, 10, 12). This may be due to the number of oncogenic partners MUC1 has been shown to interact with, namely  $\beta$ -catenin, src, and EGFR (reviewed in ref. 8). This mimetic peptide is designed to block interactions among MUC1,  $\beta$ -catenin, and EGFR, and we have shown that PMIP treatment does block MUC1 interactions with these proteins. In addition, we observed a loss of MUC1 expression in response to PMIP treatment under certain conditions, which may be the result of down-regulation of EGFR. Although the mechanism of MUC1 loss is unknown, it would certainly result in a loss of Muc1-dependent oncogenic signaling. It is tempting to speculate that in the presence of PMIP, MUC1 and EGFR are alternatively trafficked and enter the lysosomal degradation pathway, leading to their enhanced degradation. PMIP treatment of MDA-MB-231 cells overexpressing MUC1 under a cytomegalovirus promoter for only 3 hours in culture induces a loss of MUC1 overexpression, indicating that the effect is not

transcriptionally regulated (data not shown). Future studies will focus on determining the precise mechanism by which PMIP suppresses protein expression and tumor progression.

One important observation is the lack of toxicity associated with PMIP treatment (no weight loss, signs of distress, or organ failure). Whereas this is not an unexpected result with the use of an endogenous peptide, it points to a potentially low level of toxicity in patients. We have also examined the possibility that PMIP has activated an immune response in the immune-intact MMTV-pyV mT transgenic animals. Examining leukocytic infiltrates using protein levels of CD45 as a marker, we found no increase in those tumors treated with PMIP versus control (ref. 33; data not shown). Additionally, studies by groups investigating the potential adjuvant activity of the protein transduction domain have found that the TAT protein transduction domain is not immunogenic (34). One potential reason for PMIP's lack of toxicity may be the relatively fast clearance of small peptides from the body (35). Importantly, whereas PMIP-FITC appeared to be cleared overall from the body 4 hours after injection, it was retained in specific organ sites, including the mammary gland and the colon. This site-specific retention may be due to an increase in peptide-binding partners in these particular tissues.

We have previously shown that MUC1 inhibits the ligand-dependent degradation of EGFR, resulting in enhanced receptor stability (9). Furthermore, we have shown that this interaction

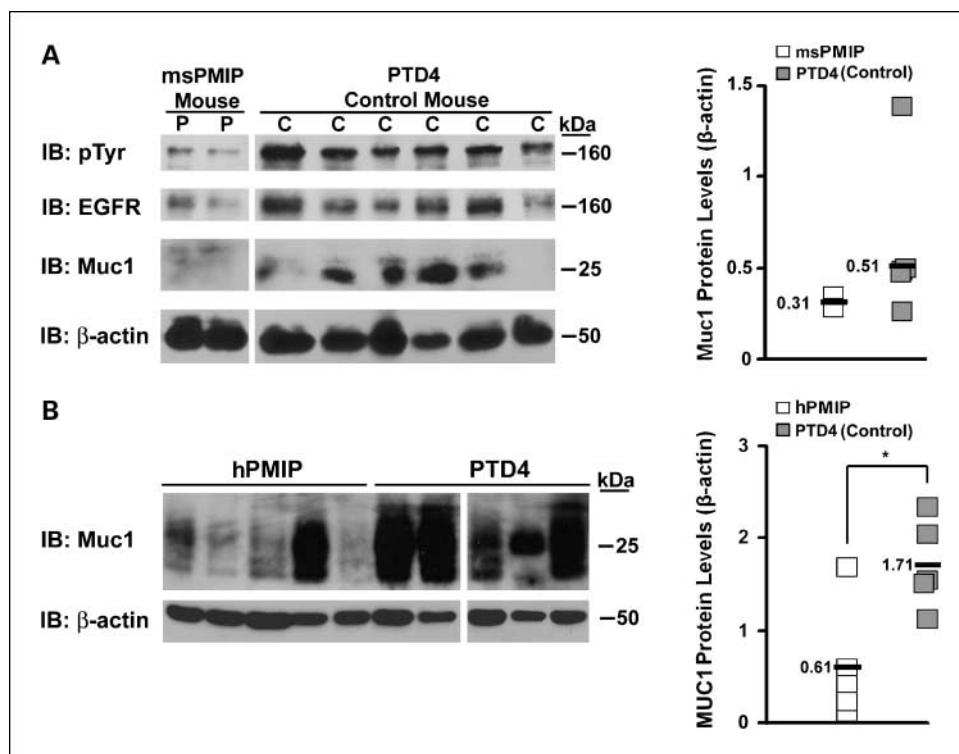


**Fig. 7.** PMIP is associated with reduced Muc1 expression. *A*, a representative MMTV-*pyW* mT msPMIP (P) treated mouse and a PTD4 mouse (C) were each injected 30 min prior to sacrifice with EGF (1  $\mu$ g/g body weight) and with peptide. Following sacrifice, the tumors were collected and protein lysates were generated. Protein (50  $\mu$ g) was separated by SDS-PAGE, transferred and immunoblotted for expression of phosphotyrosine (PY99), EGFR (1005), Muc1 (CT2), and  $\beta$ -actin (AC-15). *B*, lysates from MDA-MD-231 xenograft tumors (not treated with EGF; described in Fig. 2) were similarly analyzed to determine levels of EGFR and MUC1 protein expression. Relative protein levels of Muc1 were measured by densitometry and graphed (Muc1/ $\beta$ -actin; \*,  $P = 0.014$ , ANOVA). Molecular weights are shown on the right. IB, immunoblot. White lines through blots indicate same gel and exposure but were noncontiguous.

promotes the oncogenic properties of EGFR (9). Neither of the mouse models used in these experiments was previously shown to be dependent upon EGFR for progression, and yet, PMIP is significantly effective in each model. This indicates that PMIP may have broad applications against tumors overexpressing MUC1, which encompasses most epithelial neoplasias (36). In addition, PMIP may serve as an important adjuvant therapy with anti-EGFR treatments (reviewed in ref. 37). Our data indicate that MUC1 induces the internalization, altered trafficking, and enhanced signaling of EGFR (9). Therefore, if PMIP blocks these interactions, anti-EGFR therapy that relies on surface localization of EGFR could be enhanced by PMIP codelivery.

This study shows the efficacy of PTD4-linked peptide-based drugs and the value of MUC1-directed targets in breast cancer. Importantly, these data indicate that PMIP is a potent drug that is active at all stages of tumor progression, inhibiting growth, inducing regression, and inhibiting metastatic spread.

#### Disclosure of Potential Conflicts of Interest

No potential conflicts of interest were disclosed.

#### Acknowledgments

We thank Jamie Bitler, Jeanne Louderbough, Rachid el Bejjani, and Jose Lopez for editing of the manuscript.

#### References

- Hilkens J, Vos HL, Wesseling J, et al. Is episialin/MUC1 involved in breast cancer progression? *Cancer Lett* 1995;90:27–33.
- Zotter S, Hageman PC, Lossnitzer A, Mooi WJ, Hilgers J. Tissue and tumor distribution of human polymorphic epithelial mucin. *Cancer Res* 1988;11–12: 55–101.
- Brossart P, Schneider A, Dill P, et al. The epithelial tumor antigen MUC1 is expressed in hematological malignancies and is recognized by MUC1-specific cytotoxic T-lymphocytes. *Cancer Res* 2001;61: 6846–50.
- Takahashi T, Makiguchi Y, Hinoda Y, et al. Expression of MUC1 on myeloma cells and induction of HLA-unrestricted CTL against MUC1 from a multiple myeloma patient. *J Immunol* 1994;153:2102–9.
- Teruya-Feldstein J, Donnelly GB, Goy A, et al. MUC-1 mucin protein expression in B-cell lymphomas. *Appl Immunohistochem Mol Morphol* 2003; 11:28–32.
- Schroeder JA, Masri AA, Adriance MC, et al. MUC1 overexpression results in mammary gland tumorigenesis and prolonged alveolar differentiation. *Oncogene* 2004;23:5739–47.
- Ren J, Agata N, Chen D, et al. Human MUC1 carcinoma-associated protein confers resistance to genotoxic anticancer agents. *Cancer Cell* 2004;5: 163–75.
- Hollingsworth MA, Swanson BJ. Mucins in cancer: protection and control of the cell surface. *Nat Rev Cancer* 2004;4:45–60.
- Pochampalli MR, el Bejjani RM, Schroeder JA. MUC1 is a novel regulator of ErbB1 receptor trafficking. *Oncogene* 2007;26:1693–701.
- Pochampalli MR, Bitler BG, Schroeder JA. Transforming growth factor  $\alpha$  dependent cancer progression is modulated by Muc1. *Cancer Res* 2007;67: 6591–8.
- Li Y, Ren J, Yu W, et al. The epidermal growth factor receptor regulates interaction of the human DF3/MUC1 carcinoma antigen with c-Src and  $\beta$ -catenin. *J Biol Chem* 2001;276:35239–42.
- Schroeder JA, Adriance MC, Thompson MC, Camenisch TD, Gendler SJ. MUC1 alters  $\beta$ -catenin-dependent tumor formation and promotes cellular invasion. *Oncogene* 2003;22:1324–32.
- Yamamoto M, Bharti A, Li Y, Kufe D. Interaction of the DF3/MUC1 breast carcinoma-associated antigen and  $\beta$ -catenin in cell adhesion. *J Biol Chem* 1997; 272:12492–4.
- Li Y, Bharti A, Chen D, Gong J, Kufe D. Interaction of glycogen synthase kinase 3 $\beta$  with the DF3/MUC1 carcinoma-associated antigen and  $\beta$ -catenin. *Mol Cell Biol* 1998;18:7216–24.
- Li Y, Kuwahara H, Ren J, Wen G, Kufe D. The c-Src tyrosine kinase regulates signaling of the human DF3/MUC1 carcinoma-associated antigen with GSK3  $\beta$  and  $\beta$ -catenin. *J Biol Chem* 2001;276:6061–4.
- Schroeder JA, Thompson MC, Gardner MM, Gendler SJ. Transgenic MUC1 interacts with epidermal growth factor receptor and correlates with mitogen-activated protein kinase activation in the mouse mammary gland. *J Biol Chem* 2001;276:13057–64.

17. Schroeder JA, Troyer KL, Lee DC. Cooperative induction of mammary tumorigenesis by TGF $\alpha$  and Wnts. *Oncogene* 2000;19:3193–9.
18. Polakis P. Wnt signaling and cancer. *Genes Dev* 2000;14:1837–51.
19. He TC, Sparks AB, Rago C, et al. Identification of c-MYC as a target of the APC pathway. *Science* 1998;281:1509–12.
20. Shtutman M, Zhurinsky J, Simcha I, et al. The cyclin D1 gene is a target of the  $\beta$ -catenin/LEF-1 pathway. *Proc Natl Acad Sci U S A* 1999;96:5522–7.
21. Tetsu O, McCormick F.  $\beta$ -catenin regulates expression of cyclin D1 in colon carcinoma cells. *Nature* 1999;398:422–6.
22. Tsukamoto AS, Grosschedl R, Guzman RC, Parslow T, Varmus HE. Expression of the int-1 gene in transgenic mice is associated with mammary gland hyperplasia and adenocarcinomas in male and female mice. *Cell* 1988;55:619–25.
23. Michaelson JS, Leder P.  $\beta$ -catenin is a downstream effector of Wnt-mediated tumorigenesis in the mammary gland. *Oncogene* 2001;20:5093–9.
24. Schroeder JA, Adriance MC, McConnell EJ, Thompson MC, Pockaj BA, Gendler SJ. ErbB/ $\beta$ -catenin complexes are associated with human infiltrating ductal breast and MMTV-Wnt-1 and MMTV-c-neu transgenic carcinomas. *J Biol Chem* 2002;277:22692–8.
25. Guy CT, Cardiff RD, Muller WJ. Induction of mammary tumors by expression of polyomavirus middle T oncogene: a transgenic mouse model for metastatic disease. *Mol Cell Biol* 1992;12:954–61.
26. Spicer AP, Duhig T, Chilton BS, Gendler SJ. Analysis of mammalian MUC1 genes reveals potential functionally important domains. *Mamm Genome* 1995;6:885–8.
27. Ho A, Schwarze SR, Mermelstein SJ, Waksman G, Dowdy SF. Synthetic protein transduction domains: enhanced transduction potential *in vitro* and *in vivo*. *Cancer Res* 2001;61:474–7.
28. Wadia JS, Dowdy SF. Transmembrane delivery of protein and peptide drugs by TAT-mediated transduction in the treatment of cancer. *Adv Drug Deliv Rev* 2005;57:579–96.
29. Mosmann T. Rapid colorimetric assay for cellular growth and survival: application to proliferation and cytotoxicity assays. *J Immunol Methods* 1983;65:55–63.
30. Webster MA, Hutchinson JN, Rauh MJ, et al. Requirement for both Shc and phosphatidylinositol 3' kinase signaling pathways in polyomavirus middle T-mediated mammary tumorigenesis. *Mol Cell Biol* 1998;18:2344–59.
31. Maglione JE, Moghanaki D, Young LJ, et al. Transgenic polyoma middle-T mice model premalignant mammary disease. *Cancer Res* 2001;61:8298–305.
32. Lin EY, Jones JG, Li P, et al. Progression to malignancy in the polyoma middle T oncoprotein mouse breast cancer model provides a reliable model for human diseases. *Am J Pathol* 2003;163:2113–26.
33. Trivedi P, Cuomo L, Christensson B, et al. Augmentation of leukocyte infiltration in murine tumors expressing B-cell derived but not nasopharyngeal carcinoma derived EBV membrane protein LMP1. *J Med Virol* 2000;60:417–24.
34. Kittiworakarn J, Lecoq A, Moine G, et al. HIV-1 Tat raises an adjuvant-free humoral immune response controlled by its core region and its ability to form cysteine-mediated oligomers. *J Biol Chem* 2005;281:3105–15.
35. Torchilin VP, Lukyanov AN. Peptide and protein drug delivery to and into tumors: challenges and solutions. *Drug Discov Today* 2003;8:259–66.
36. Packer LM, Williams SJ, Callaghan S, Gotley DC, McGuckin MA. Expression of the cell surface mucin gene family in adenocarcinomas. *Int J Oncol* 2004;25:1119–26.
37. Dassonville O, Bozec A, Fischel JL, Milano G. EGFR targeting therapies: monoclonal antibodies versus tyrosine kinase inhibitors. Similarities and differences. *Crit Rev Oncol Hematol* 2007;62:53–61.